

Article

Investigation of Cooling Techniques for Roof-Mounted Silicon Photovoltaic Panels in the Climate of the UAE: A Computational and Experimental Study

Tarek Abdelaty ¹, Hassam Nasarullah Chaudhry ^{1,*}  and John Kaiser Calautit ² 

¹ Department of Architectural Engineering, School of Energy, Geoscience, Infrastructure and Society, Heriot-Watt University, Dubai P.O. Box 38103, United Arab Emirates; ta64@hw.ac.uk

² Department of Architecture and Built Environment, University of Nottingham, Nottingham NG7 2RD, UK; john.calautit1@nottingham.ac.uk

* Correspondence: h.n.chaudhry@hw.ac.uk

Abstract: The increased adoption of photovoltaic (PV) systems for global decarbonisation necessitates addressing the gap in reduced panel efficiency due to overheating. This issue is especially prominent in countries with extremely hot and humid climates where PV utilisation is hindered by declining panel output. A systematic review of PV cooling techniques suggests passive systems are more economical, sustainable, and easier to implement than active systems, despite possessing a lower cooling potential. Air-based systems were deemed the most viable for the UAE's climate, considering both performance and cost. Based on these findings, two individual improvements for air-based cooling systems were combined in an attempt to achieve greater cooling: a segmented multiangular aluminium fin heatsink developed from previous works. Various perforation patterns were simulated on the chosen heatsink using CFD software to determine the most optimal arrangement. The original and optimised models were both tested under real-life conditions in Dubai, United Arab Emirates, revealing similar cooling potential between the two. The results of this study indicate that the PV cell temperature can be decreased by up to 10 °C with the placement of an aluminium fin heatsink, which corresponds to an approximate efficiency increase of 5%.

Keywords: photovoltaics; efficiency; passive cooling; air-based systems; aluminium fin heatsink; perforations; computational fluid dynamics; experimental investigation



Citation: Abdelaty, T.; Chaudhry, H.N.; Calautit, J.K. Investigation of Cooling Techniques for Roof-Mounted Silicon Photovoltaic Panels in the Climate of the UAE: A Computational and Experimental Study. *Energies* **2023**, *16*, 6706. <https://doi.org/10.3390/en16186706>

Academic Editors: Enrique Romero-Cadaval and Carlo Renno

Received: 7 August 2023

Revised: 12 September 2023

Accepted: 15 September 2023

Published: 19 September 2023



Copyright: © 2023 by the authors. Licensee MDPI, Basel, Switzerland. This article is an open access article distributed under the terms and conditions of the Creative Commons Attribution (CC BY) license (<https://creativecommons.org/licenses/by/4.0/>).

1. Introduction

Over the last few decades, there has been growing concern for the environment and climate change, leading to an increased adoption of renewable energy sources across various sectors. The building sector in particular, which is accountable for approximately 40% of global energy consumption and 30% of global carbon dioxide emissions [1], has been the primary target of efforts to integrate renewables. That is because it largely consists of an existing stock of energy-inefficient and high-emitting buildings, causing its progress towards the Paris Agreement target for net zero by 2050 to be generally slower than other sectors. In fact, the International Energy Agency (IEA) has described the building sector as “not on track” in its 2022 sectorial overview [2].

In accordance with climate-change reports, global green building certifications such as LEED and BREEAM, as well as local building rating systems such as Estidama in Abu Dhabi, encourage the use of renewable energy sources, both for new construction and retrofitting projects. These include solar photovoltaic (PV) panels, solar thermal collectors, wind turbines, geothermal systems, and biomass boilers. Nonetheless, PVs remain the most commonly used renewable energy source by far, per the latest Fraunhofer ISE (2022) report which states that PVs amount to a global installed capacity of 850 GWp [3]. That is because they are relatively affordable and cost-effective compared to other renewables, not

to mention that they can easily be installed on rooftops or integrated into building facades. Despite the availability of nonsilicon-based PVs such as cadmium telluride (CdTe), copper indium gallium selenide (CIGS), perovskite, and organic PVs (OPVs), Si-PV technology remains the most established and economically viable option to date, representing 95% of the market share as of 2021 [3].

Currently, the two primary types of Si-PVs panels are monocrystalline (Si-mono) and polycrystalline (Si-poly), with Si-mono being more prevalent in commercial settings due to its higher efficiency rates that range from 17% to 19% [4], as well as an average lifespan ranging from 25 to 30 years [5]. Nevertheless, one major downside of Si-PVs is the degradation of their electrical efficiency with the increase in operational temperature [6]. This depends on a multitude of meteorological factors, such as solar irradiance, ambient temperature, wind speed, and wind direction, in addition to manufacturing and installation factors, such as component materials, tilt angle, and installation geometry [7].

Si-poly PVs are generally more susceptible to overheating compared to their Si-mono counterparts due to their lower conversion efficiency. As per the photoelectric effect, only photons with energy levels at or above the 1.12 eV ($\approx 1.79 \mu\text{J}$) bandgap can result in electron release in crystalline silicon [4]. Subsequently, lower energy photons below the bandgap only serve to heat the PV cell. These mostly fall within the ultraviolet spectrum. The optimal operating temperature for achieving maximum panel efficiency (also known as the standard test condition) is 25 °C [8]. This decreases by 0.25–0.5% for every 1 °C increase in temperature [9]. The implications of this issue create a significant roadblock for the widespread implementation of Si-PV technologies. This is especially significant in the MENA region where sunlight is abundant; yet, PV panels can easily reach temperatures of up to 75 °C, which corresponds to a 25% decline in efficiency [10]. Extended exposure to such harsh weather conditions has severe impacts on the open-circuit voltage of solar panels, resulting in decreased power-conversion efficiency and irreversible cell degradation. Furthermore, the combination of high temperatures and ultraviolet radiation makes panels more vulnerable to several ageing mechanisms, including delamination, EVA discolouration and corrosion, back-sheet adhesion loss, bubbles, and cell cracks [11]. These degradation mechanisms highlight the need for cooling techniques that can increase the lifespan of PVs and help them maintain optimal efficiency throughout their lifecycle.

The aim of this research is to investigate the most effective cooling system for roof-mounted PV panels in the MENA climate and modify it with the goal of further enhancing its performance. The overall economic and environmental dimensions of the proposed system will also be considered. The aforementioned aims will be achieved through the following set of objectives:

1. Carrying out a systematic literature review to identify the most optimal PV cooling technique from existing literature;
2. Proposing a set of modifications to the selected cooling technique to increase its cooling potential;
3. Evaluating the performance of the proposed modifications using numerical analysis and identifying the model that is most viable;
4. Investigating the performance of the selected modification(s) using an experimental setup and commenting on the results.

2. Literature Review

The cooling of PV panels can be categorized into active and passive techniques. Active systems require energy input to remove heat from the panels, whereas passive systems depend on natural processes like conduction, convection, and radiation to induce cooling.

2.1. Active Cooling

Active systems typically employ fluids to capture and disperse the heat generated by PV panels. This fluid can be either air or a liquid. Air cooling involves circulating air over the panel surface using fans. Meanwhile, liquid cooling utilises water or refrigerants

circulated through a heat exchanger in contact with the panel. This absorbs and dissipates heat through a radiator and is known as an indirect active cooling system. Conversely, a direct system involves spraying water directly onto the face of the panel using nozzles. Nanofluids, made by suspending nanoparticles in a base fluid like water, are also an emerging fluid for PV cooling [12]. However, more research is needed to assess their effectiveness and economic viability.

Despite their complexity and cost, active cooling systems outperform passive cooling systems in terms of heat removal from PVs, resulting in increased power output and extended panel lifespan. Their application extends beyond conventional Si-PVs to include concentrated photovoltaics (CPVs), building integrated photovoltaics (BIPV), and photovoltaic–thermal (PV/T) systems [13]. Nižetić et al. [13] conducted a comprehensive analysis of active cooling methods, evaluating their performance, economic viability, and environmental impact. The research findings are summarised in Table 1.

Table 1. Summary of active cooling techniques [13].

Cooling technique	Efficiency increase	Increase in panel power output	Reduction in panel operating temperature
water	2.1% to 37.5%	10% to 35.5%	0.7 °C to 32 °C
water (PV/T)	2% to 22.2%	N/A	10 °C to 33 °C
air	2.6% to 10%	3% to 15%	5 °C to 30 °C
nanofluids	7% to 19.5%	20% to 30%	18 °C to 24 °C

Summarised data from [13] reveals that water-cooling systems outperform other methods, resulting in increased PV power output due to water’s higher specific heat capacity and thermal conductivity. Despite performing similarly to water, nanofluids are less appealing due to the lack of research and the complexity involved in their production. However, employing water cooling for roof-mounted PVs would have significant structural implications on buildings, especially with large-scale PV arrays.

Given the limited economic and environmental analysis in the majority of research studies, the authors in [13] performed a case study utilising a 30 kW PV system in a Mediterranean climate. This was used to calculate the levelised cost of electricity (LCOE), taking into account the initial investment and operational fuel costs of the cooling system. A life cycle analysis (LCA) of the proposed active cooling methods was carried out using Gabi Software in accordance with ISO 14040 standards.

The study by [13] concluded that all the active cooling systems assessed were not economically viable, with the LCOE for the 30 kW PV system ranging from 0.096 EUR/kWh to 0.159 EUR/kWh. Additionally, the LCA revealed that air-based cooling techniques had the most negative impact on the environment, primarily due to increased global warming and environmental acidification potential. Due to their economic and environmental shortcomings, in addition to the limitations associated with their installation in commercial buildings, active cooling techniques were dismissed as a feasible solution for tackling the issue of PV overheating.

2.2. Passive Cooling

Compared to active systems, passive cooling techniques for PV panels are typically less expensive and less complex [14]. While they may have lower cooling efficiency, they require minimal maintenance and do not entail additional costs, making them a more advantageous and economical choice compared to active systems.

A thorough literature review by Nižetić et al. [15] revealed that the majority of passive cooling methods use phase change materials (PCMs), air, liquid (water, nanofluids, etc.), and radiative cooling. An outline of the effectiveness of each cooling technique can be seen in Table 2.

Table 2. Summary of passive cooling techniques [15].

Cooling technique	Efficiency Increase	Increase in the panel Power output	Reduction in the panel Operating temperature
PCM	1.15–21.2%	4–55%	0.4–50 °C
Liquids	8.5–22%	8.8–52.6%	9–50 °C
Air	3.2–20%	7.5–50%	6–38 °C
Radiative	0.4–2.6%	Non	6–21 °C

2.2.1. Radiative Cooling

Radiative cooling employs highly reflective materials in the infrared (IR) spectrum on the backside of PVs to release absorbed heat into the surrounding environment. A study by Safi and Munday [16] investigated radiative cooling for terrestrial and low-orbit applications using numerical analysis. The proposed structure consisted of a solar cell coupled to a selective thermal emitter with a back mirror. The solar cell absorbs light above the bandgap while the radiative cooler absorbs midinfrared light and emits it back into the surrounding atmosphere. Numerical simulations yielded an efficiency increase of approximately 0.87% under standard terrestrial test conditions of 293.15 K ambient temperature, 800 W/m² solar irradiation, and roughly 1 m/s wind velocity. The PV panel efficiency was higher in near-earth-orbit conditions, ranging from 0.4% to 2.6% for the assumed operating temperatures of 293 K to 358 K. This enhanced PV efficiency in extra-terrestrial conditions can be attributed to the radiator's emission of heat over all wavelengths which results in greater heat dissipation [16].

One critical point to note is that radiative cooling is heavily influenced by atmospheric humidity—a factor not considered in the study by [16]. As such, the use of radiative cooling is limited to regions with predominantly dry climates [17]. Radiative cooling is, therefore, not suitable for the coastal areas of the MENA region, which are characterized by high levels of humidity that would render the system ineffective.

2.2.2. Phase-Change Materials

PCMs exhibit the most significant cooling potential among other passive technologies, making them an appealing option for mitigating PV overheating. Such substances can store and release large amounts of energy through phase changes, typically from solid to liquid states. This latent heat-storage mechanism enables PVs to maintain desired temperatures without the need for external energy inputs.

A study of three general types of PCM materials was carried out by Hasan et al. [18]. These included a variety of organic and inorganic PCMs, as well as eutectic mixtures. The three classes of PCMs investigated by [18] comprised salt hydrates (SP22 and CaCl₂·6H₂O), paraffin wax (RT22), eutectic mixtures of fatty acids (capric–lauric acid (CL), and capric–palmitic acid (CP)), with a total of five different PCMs. The thermophysical properties of the chosen PCMs were evaluated in relation to the PV standard test condition (STC) of 25 °C. The study determined that CaCl₂·6H₂O, SP22, and RT20 PCMs were not effective in regulating PV temperatures. On the other hand, the eutectic mixtures of fatty acids (CL and CP) exhibited higher heats of fusion, as well as melting and solidification temperature ranges between 19 and 25 °C, despite their very low thermal conductivities. This made them more suitable for PV cooling applications. Of both CL and CP, CP had a melting point closer to the PV control temperature, as well as a higher heat of fusion than CL, making it the most optimal choice for PV temperature regulation [18].

Considering that capric–palmitic acid (CP) is derived from abundant natural sources such as coconut oil, palm kernel oil, and animal fats, it is generally inexpensive and easy to produce [19]. Nevertheless, the fact that it is an organic PCM means that it will not withstand frequent thermal cycling and will quickly suffer from chemical degradation [20]. Additionally, building owners will still have to contend with the problem of sealing issues [20]. Sealing issues are critical not only because they can impair the system's effectiveness but also because they can pose a safety hazard. This is especially true for CP,

given that it contains oils and animal fats which pose a fire risk, especially since it will be subjected to high temperatures. Supposing that all these issues are addressed, CP would still not be guaranteed to be very effective under realistic climate conditions in MENA regions as temperatures will mostly be higher than 25 °C. In view of all these shortcomings, PCMs were deemed impractical for PV cooling.

2.2.3. Liquid-Based Cooling

Liquid-based cooling relies on immersing PV panels in a liquid-filled container, which may be open or closed. The liquids used include dimethyl silicon oil, ethylene glycol, and water (which is the most common option).

A numerical and experimental study of liquid immersion was carried out by Tina et al. [21] in a Mediterranean climate. The authors investigated the optical and thermal behaviour of Si-mono PV panels submerged in shallow water at varying depths, ranging from 1 to 15 cm. This research involved analysing various phenomena, including irradiance absorption, reflection, and refraction at the air–water boundary, as well as the panels' spectral response. The study revealed a 15% enhancement in PV output at a depth of 4 cm, highlighting the significance of water depth for optical losses and panel performance. Nevertheless, the study did not investigate the potential long-term effects of submersion on panel lifespan or evaluate the economic and environmental implications of this cooling technique.

Another study conducted by Abdulgafar et al. [22] investigated a 15 m² Si-poly PV cell submerged in distilled water in a Middle Eastern climate. The panel's power output was measured at depths of 1 to 7 cm. The results indicated a maximum energy conversion efficiency of 22% at a depth of 6 cm. However, the paper did not discuss any correlations between water quality and performance improvement, nor did it include economic or environmental assessments of the cooling method.

Lastly, Al-Amri et al. [23] evaluated the operating temperature of PV panels in a Middle Eastern climate when submerged in engine oil, ethylene glycol and regular water. The liquid-immersion technique was used in combination with an active cooling system consisting of heat pipes connected to a chiller. The chiller's evaporator was used to cool the heat pipe's condensation section, thus increasing its thermal efficiency. Of the three liquids examined, water demonstrated the greatest temperature reduction, with a maximum drop of 53% corresponding to a 13% increase in open-circuit voltage. As with the two previous studies, no analysis of economic or environmental aspects was undertaken.

While liquid immersion significantly enhances PV performance, it remains difficult to implement due to substantial structural implications, especially for large-scale arrays of roof-mounted PVs [15]. Furthermore, the need for periodic transportation and replacement of water to maintain adequate depth and purity would result in significant logistical and maintenance requirements, rendering the solution very costly and time-consuming. It was subsequently recognized that liquid-based PV cooling would be ineffective under MENA conditions, especially given the water scarcity in the region.

2.2.4. Air-Based Cooling

Air-based cooling is commonly achieved through the use of metal fins attached to the back of PV panels. That is because the panel's backside is closest to the actual cell temperature, making it the best surface through which heat can be dissipated [9]. Aluminium is the prevalent material of choice for fin heatsinks, given its high thermal conductivity, light weight, versatility, and affordability. Grubisic-Cabo et al. [24] concluded that, in order for effective cooling to occur, the fins need to act on as much of the PV panel's backside as possible. If correctly designed and computer-simulated, an aluminium fin (Al-fin) heatsink can promote turbulent natural convection and allow for greater heat exchange. The fins would essentially serve as an extension of the absorber plate, thereby increasing its surface area for greater heat dissipation [17]. Nonetheless, it is crucial to optimise the surface area of the fin heatsink to balance the rate of heat dissipation and manufacturing cost.

In addition to the design of the heatsink, the placement of the fins in relation to the incoming wind is also of great importance. A study by Nižetić et al. [9] showed that in the case of PV panels without fins, the average PV panel temperature depends largely on the wind angle of attack, resulting in temperature variations of up to 5 °C. The authors also identified a very important phenomenon wherein warm air accumulates at the lower and upper edge of the backside sections of the PV panel, leading to the creation of a hot-air bubble. This hot-air bubble essentially insulates the back sheet from ambient air, resulting in the decline of panel efficiency. The presence of this inherent phenomenon demands the application of fin heatsinks so as to create a heat-conduction bridge across this flow-separation bubble, thereby counteracting its formation.

Grubisic-Cabo et al. [25] experimentally investigated an Al-fin heatsink mounted to the back of a 50 W Si-poly panel using epoxy conductive glue. Conductive glue is an essential component of fin heatsinks as it thermally links the Al-fins with the back of the panel. Testing was carried out in ambient temperatures of 12 °C in the city of Split, Croatia. The study compared two Al-fin heatsinks that were initially optimised using Ansys computational fluid dynamics (CFD). The first heatsink consisted of a set of linear L-profiles placed in parallel while the second consisted of a set of randomly positioned L-profiles with perforations (see Figure 1). A third referent panel without any modifications was used as a control. To further ensure the accuracy of the results, referent measurements were first obtained for the two panels on which the heatsinks were to be applied. This was done to detect the general difference between the output of the two panels as a result of imperfections from the manufacturing process as well as any ageing mechanisms.



Figure 1. Linear and random perforated fins [25].

The randomly positioned fins were found to have better performance compared to the fins placed in parallel, yielding an average efficiency improvement of around 2%. This was attributed to the randomised arrangement of fins—given that air actually flows from all directions in realistic conditions—as well as the introduction of perforations which increased air penetration through the heatsink. In the case of higher wind speeds, the increase in efficiency was stochastic in nature for the optimised model. Conversely, in the absence of wind, the heatsink neither increased power yield nor negatively impacted the PV panel's electrical efficiency. It was also found that the effect of fin thickness and thermal conductivity was negligible since heat exchange primarily depends on the surface area of the fins. The most notable feature of this study was the introduction of perforations into the fin geometry as it significantly improved airflow. Nevertheless, while perforations facilitate airflow, they reduce the surface area available for heat transfer and should therefore be utilised carefully so as to not compromise the fins' performance [7].

The topic of perforations was further investigated by Nazari and Eslami [7] through a numerical study that utilised CFD (ANSYS Fluent 19) to evaluate the cooling potential of different perforation patterns integrated into the aluminium frame of Si-mono PV panels. The authors assessed the airflow, temperature distribution, and power output of

the proposed perforations for an equivalent heat-flux value of 600 W/m^2 in both forced convection (wind velocity of 4 m/s) and natural convection (zero wind velocity) scenarios. The numerical results indicated that frame perforations are effective for natural convection, with a 3.8 K temperature reduction observed in the best-case scenario, whereas the average PV temperature in forced convection remained nearly unchanged. A similar study by Abd-Elhady et al. [10] observed $8 \text{ }^\circ\text{C}$ of cooling in the numerical simulation of a naturally ventilated Si-mono PV by creating nine holes of 1 mm diameter between cells. This is substantiated by another study carried out by Marinić-Kragić et al. [26], where the introduction of slits in the PV panel surface yielded maximum temperature reductions of $3 \text{ }^\circ\text{C}$ for wind speeds up to 5 m/s . It is, therefore, reasonable to conclude that frame perforations do not significantly affect the panel temperature, as opposed to perforations that are in closer proximity to the PV cells themselves. As a matter of fact, a study by Nižetić et al. [27] already supports this conclusion.

A fin heatsink covering more of the panel's backside was developed by Hernandez-Perez et al. [28]. The authors investigated a multiangular segmented fin profile consisting of non-perforated Al-fins (see Figure 2). These were placed at alternating angles of $\pm 30^\circ$ to the vertical axis, with 20 mm gaps in between to allow for uniform airflow. The developed heatsink was compared against a conventional heatsink with linear fins at 90° , similar to Figure 1. A numerical analysis was first performed on both models using ANSYS Fluent, after which both heatsinks were experimentally tested on two 15 W Si-Poly panels in a Latin American climate.

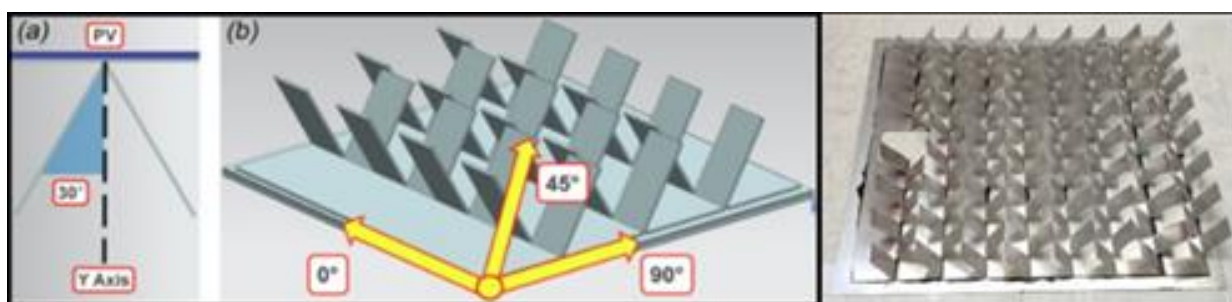


Figure 2. Multiangular segmented fin heatsink model developed by Hernandez-Perez et al. [28].

The segmented heatsink developed by [28] was found to reach a relatively homogeneous temperature distribution compared to the conventional, linear profile. Numerical simulation results showed improvements in temperature homogenisation across the panel, with a maximum reduction of $9.4 \text{ }^\circ\text{C}$. Experimental results were in close congruence with the CFD model, with the heatsink achieving a reduction of around $10 \text{ }^\circ\text{C}$ during peak irradiance (970 W/m^2). This reduction in temperature corresponds to an improvement in the electrical conversion efficiency of the system by roughly 4% , based on the fact that panel efficiency decreases by $0.25\text{--}0.5\%$ for every $1 \text{ }^\circ\text{C}$ increase in temperature above the STC. By adopting a multiangular configuration, the system was able to maintain a stable thermal response across different directions of airflow, which ranged from 2.7 to 4.5 m/s at 0° , 45° , and 90° , although the cooling effect was greatest when the air hit the wider face of the fins. One observation highlighted by the authors in [28] was that increasing the length of the fins results in an exponential decrease in their thermal efficiency as less heat is transmitted when moving away from the base of the fins.

Lastly, a CFD study by Mankani et al. [29] evaluated the efficiency of copper as an alternative heatsink material to aluminium, considering that copper is more thermally conductive. Copper has a thermal conductivity of about 401 W/mK , whereas aluminium has a thermal conductivity of about 237 W/mK , meaning that copper is better at dissipating heat than aluminium. The study arrived at the conclusion that copper is a more effective heatsink material as it allows for greater heat exchange. Although both aluminium and copper heatsinks exhibited a uniform temperature reduction, the copper heatsink was able

to dissipate between 2.3% and 2.4% more heat. It is worth noting that the study did not consider the economic factors of using copper as a heatsink material. While the price of copper depends on a variety of factors, such as location, market demand, and availability, it is typically around three to four times more expensive than aluminium [30]. In other words, the cost of cooling one solar panel using a copper heatsink can be used to cool at least three identical solar panels using the exact same heatsink. Moreover, while the CFD results obtained may be promising, copper heatsinks may or may not perform at the same expected level under realistic conditions. A comprehensive cost analysis and experimental investigation are therefore necessary to develop a rationale for the implementation of copper heatsinks.

Overall, the systematic review of existing literature indicated that air-based passive cooling—particularly Al-fin heatsinks—was the most suitable option for roof-mounted PV applications in the MENA region, both in terms of performance and cost.

3. Proposed Fin Configuration

Based on the extensive review of recent advancements in the field of air-based passive cooling, the choice was made to adopt the aluminium fin heatsink developed by Hernandez-Perez et al. [28] as the foundation for the proposed model. The two main reasons behind this heatsink's selection were the fact that it effectively covers much of the panel's backside as well as the fact that its segmented and angled fins allow it to maximise the contact area with incoming air from multiple directions. In doing so, this heatsink ensures equal heat dissipation across the entire PV surface, thereby addressing the current-matching problem described by Bahaidarah et al. [31]. Furthermore, it provides enough flexibility for implementation across different geographical areas with different prevailing wind directions. Since the panels have to be oriented to face south by default, it is crucial for the utilised heatsink to be capable of adapting to any angle of wind attack.

Despite its optimised performance, it was still believed that there was room for improvement in the heatsink's performance, namely through the introduction of perforations. While the existing literature on the effect of perforations in PV cooling is slightly inconsistent, casting doubts on the perforations' ability to have a sizeable impact on panel temperature, the concept itself seems to have some potential (at least theoretically speaking). Furthermore, given that Grubišić-Čabo et al. [25] was the only study to introduce perforations into Al-fins rather than the panel structure, in addition to the fact that it yielded positive results, there is reason to believe that it may actually be overlooked as a viable enhancement. Nevertheless, the contribution of the perforations towards the performance improvement was unclear since its effect was not isolated, which provides more reasons to investigate perforations further.

Given the limited number of studies investigating perforations, as well as the lack of experimentation with different perforation shapes and patterns, this study took the liberty to propose a multitude of different design configurations to be applied to the selected heatsink. The dimensions and spacing of these perforation patterns were dictated by the available area on each fin which, in turn, was determined by the size of the PV panel that was to be used for the experimental investigation. Considering that this study used a panel of dimensions 67.5 cm × 52.5 cm, as opposed to the ones used by Hernandez-Perez et al. [28] which had dimensions of 35 cm × 36 cm, the dimensions of the fins proposed by the author had to be adjusted slightly in order to ensure fit.

For comparison, the Al-fin heatsink used in the original study consisted of 0.71 mm thick fins that were 40 mm in length and 20 mm in width (16 fins per profile), each at an interleaved inclination of $\pm 30^\circ$ with respect to the vertical axis, whereas the adjusted Al-fin heatsink used for this study consisted of 0.71 mm thick fins that were 85 mm in length and 34 mm in width (13 fins per profile) at the same inclination of $\pm 30^\circ$. The reason why the fin length was significantly increased for this study was to account for the recess on the back of the available panel, which was roughly 35 mm in depth, as well as the slightly greater width of the fins. Additionally, a section of the heatsink was left open to make way

for the junction box located at the top centre of the panel, similar to the photograph of the physical heatsink shown in Figure 2. The seven different perforation patterns developed for this study can be seen within the schematic information shown in Figures 3 and 4. This schematic diagram provides an overview of the heatsink modelling and data-analysis process that was followed by this study to arrive at the optimal fin-perforation pattern yielding the greatest temperature reduction.

4. Computational Study

4.1. Simulation Methodology

The 3D panel and fin geometries were modelled using AUTODESK Inventor 2023. While detailed models were initially developed where every fin profile was added as a separate element, these models were replaced with simplified models where all the fins were combined into a single entity.

The law of mass conservation equation is that the mass of a controlled volume will remain constant, regardless of any process acting inside the system. The controlled system can change form but cannot be destroyed. The general form (Equations (1) and (2)) of the partial differential equation of the continuity equation can be written as follows:

$$\frac{\partial \rho}{\partial t} + \nabla \cdot (\rho \vec{v}) = S_m \quad (1)$$

where:

$$\nabla = \frac{\partial}{\partial x} + \frac{\partial}{\partial y} + \frac{\partial}{\partial z} \quad (2)$$

S_m is the mass added to the continuous phase from the dispersed second phase and any user-defined sources.

Newton's second law states that the rate of change of momentum of a fluid particle equals the sum of the forces acting on it. In this case, there are two types of forces acting on the fluid particles, including body forces (gravity, centrifugal, and electromagnetic) and surface forces (pressure, viscous, shear, and normal). The rate of increase of (x, y, z) momentum per unit volume of a fluid particle is given by:

$$\rho \frac{Du}{Dt}, \quad \rho \frac{Dv}{Dt}, \quad \rho \frac{Dw}{Dt}$$

where ρ is the density of the fluid. Based on this principle, the momentum conservation equation can be written as follows. The x component of the momentum equation is found by setting the rate of change of the x momentum of the fluid particle equal to the total force in the x direction on the element due to surface stresses and the rate of increase of x -momentum due to sources, as formulated in Equation (3).

$$\rho \frac{Du}{Dt} = -\frac{\partial p}{\partial x} + \frac{\partial \tau_{xx}}{\partial x} + \frac{\partial \tau_{yx}}{\partial y} + \frac{\partial \tau_{zx}}{\partial z} \quad (3)$$

Similarly, the y component of the momentum equation is formulated in Equation (4),

$$\rho \frac{Dv}{Dt} = -\frac{\partial p}{\partial y} + \frac{\partial \tau_{xy}}{\partial x} + \frac{\partial \tau_{yy}}{\partial y} + \frac{\partial \tau_{zy}}{\partial z} \quad (4)$$

while the z component of the momentum equation is formulated in Equation (5).

$$\rho \frac{Dw}{Dt} = -\frac{\partial p}{\partial z} + \frac{\partial \tau_{xz}}{\partial x} + \frac{\partial \tau_{yz}}{\partial y} + \frac{\partial \tau_{zz}}{\partial z} \quad (5)$$

The standard k - ϵ transport model [32], which is frequently used for incompressible flows, was used to define the turbulence kinetic energy and flow dissipation rate within the model. The use of the standard k - ϵ transport model on cylindrical pipe flows has been

found in previous works [33]. The turbulence kinetic energy, k , and its rate of dissipation, e , are obtained from the following transport equations formulated in Equations (6) and (7).

$$\frac{\partial}{\partial t}(\rho k) + \frac{\partial}{\partial x_i}(\rho k u_i) = \frac{\partial}{\partial x_j} \left[\left(\mu + \frac{\mu_t}{\sigma_k} \right) \frac{\partial k}{\partial x_j} \right] + G_k + G_b - \rho \epsilon - Y_M \quad (6)$$

$$\frac{\partial}{\partial t}(\rho e) + \frac{\partial}{\partial x_i}(\rho e u_i) = \frac{\partial}{\partial x_j} \left[\left(\mu + \frac{\mu_t}{\sigma_e} \right) \frac{\partial e}{\partial x_j} \right] + C_{1e} \frac{e}{k} (G_k + C_{3e} G_b) - C_{2e} \rho \frac{e^2}{k} \quad (7)$$

where G_k represents the generation of turbulence kinetic energy due to the mean velocity gradients, and G_b represents the generation of turbulence kinetic energy due to buoyancy. Y_M represents the contribution of fluctuating dilatation in compressible turbulence to the overall dissipation rate. C_{1e} , C_{2e} , and C_{3e} are constants, σ_k and σ_e are the turbulent Prandtl numbers for k and e .

The energy equation is derived from Newton's first law, which states that the rate of change of energy inside a fluid element is equal to the rate of heat added to the fluid element and the work done on the fluid element. The energy equation used in this study can be written as formulated in Equation (8).

$$\frac{\partial}{\partial t}(\rho E) + [\vec{v}(\rho E + p)] = \nabla[k_{eff} \nabla T - \sum_j h_j \vec{J}_j + (\overline{\tau_{eff}} \times \vec{v})] + S_h \quad (8)$$

where k_{eff} is the effective conductivity, \vec{J}_j is the diffusion heat flux of species j , and S_h includes the heat of the chemical reaction and other volumetric heat sources that are user defined.

The different layers constituting the PV were also modelled as a single entity with a thickness of 3.6 mm. This was done to avoid any meshing issues related to contact regions and small edges. The models were then imported into the built-in CFD tool for simulation. The solid geometries were enclosed in computational domains that were sized with respect to panel length (0.635 m) based on the sizing approach outlined by Nazari and Eslami [7] in their CFD section. The fluid domain length was ninefold the length of the panels, with a third of this length being from the inlet to the panel. Meanwhile, domain height and width were both sevenfold the panel length. The panel was placed at an inclination angle of 24° and rotated such that the air from the velocity inlet would approach the fins at 45° . These orientations corresponded to the actual conditions under which the panel would be placed in the experimental setting. Additionally, the panel was placed at a height of 0.5 m above ground. The computational domain was assigned as air while the panel frame and heatsink fins were assigned as aluminium. Since it was modelled as a single element, a custom material was created for the equivalent layer, which consists of the PV cell, back sheet, and glass. The thermal and physical properties of this layer were also taken from Nazari and Eslami [7] and can be seen in Figure 3.

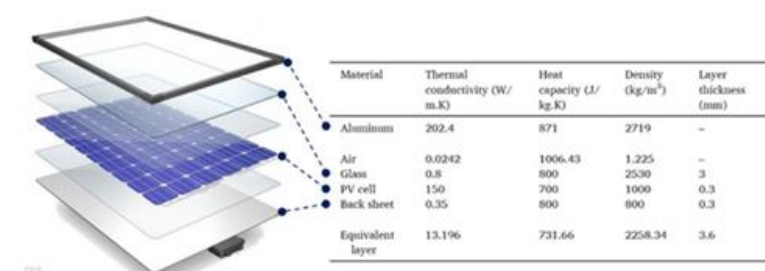


Figure 3. Thermal and physical properties of the equivalent layer.

Figure 4 displays the schematic of the heatsink modelling and data-analysis process which was used to arrive at the optimal fin-perforation pattern. Following this, the bound-

ary conditions were assigned to the air inlet, pressure outlet, and panel face. The air inlet was assigned a velocity of 2 m/s and a temperature of 28 °C while the pressure outlet was assigned a pressure value of 0 Pa. These boundary conditions were adopted from the numerical analysis carried out by Hernandez-Perez et al. [28]. To simulate the incoming irradiance, the panel was assigned a heat flux of 700 W/m². Finally, the auto-sizing tool was used for mesh sizing and the steady-state CFD simulations were run until convergence for all the models under the following settings (Table 3).

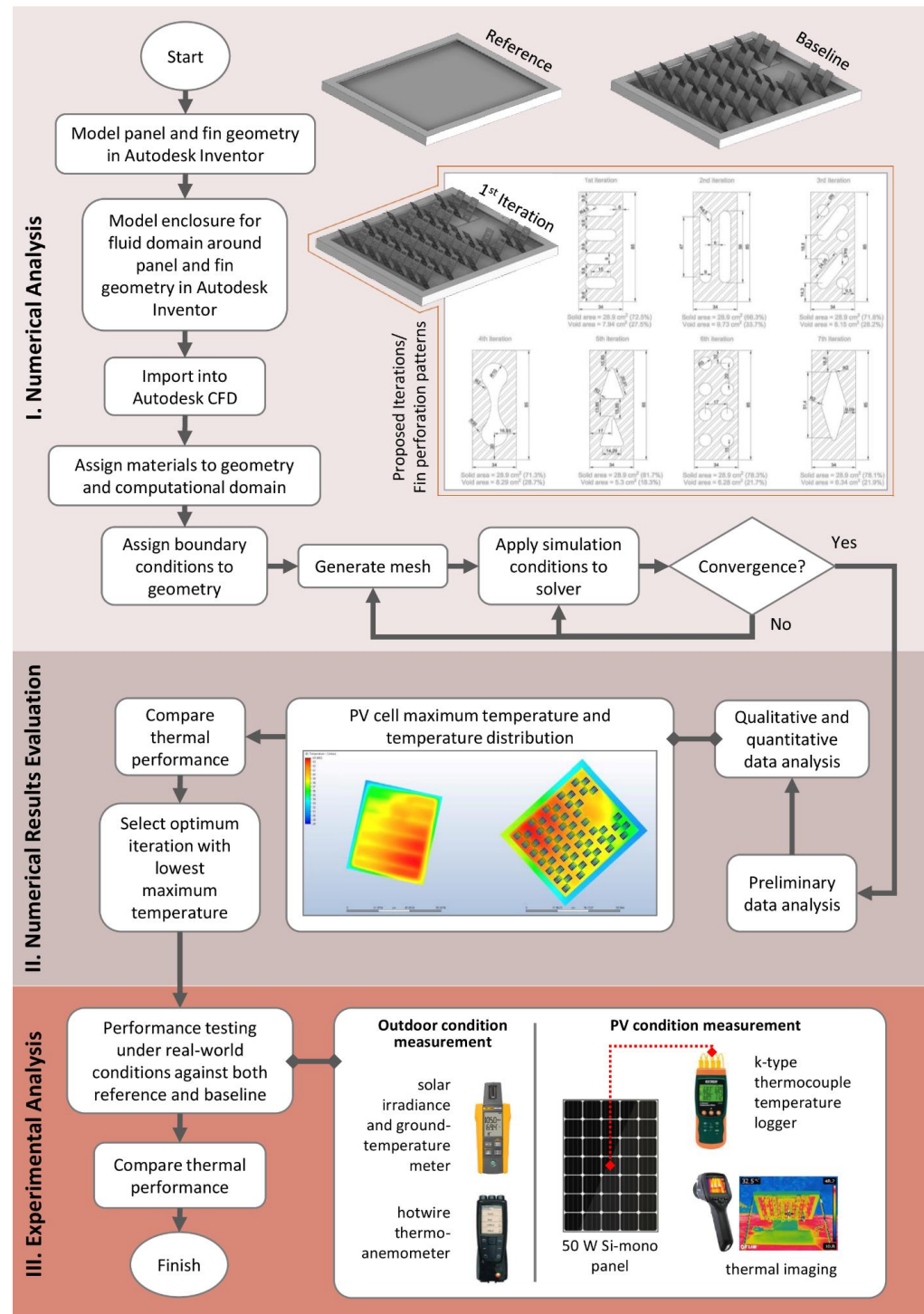


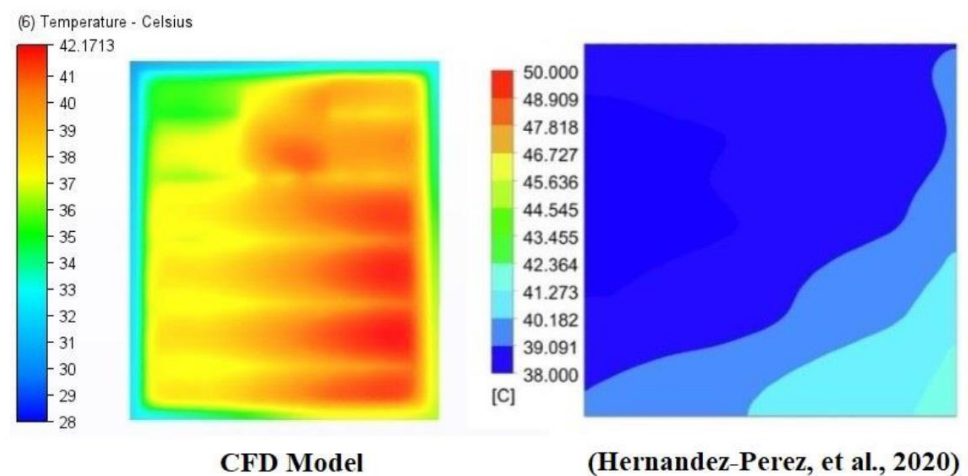
Figure 4. Schematic of the heatsink modelling and data-analysis process for fins optimisation.

Table 3. Numerical model boundary conditions.

Physics	Flow	Yes
	Compressibility	Incompressible
	Hydrostatic pressure	No
	Heat transfer	Yes
	Auto forced convection	No
	Radiation	Yes
	Gravity method	Earth
	Gravity direction (x, y, z)	0, −1, 0
Turbulence	Laminar/Turbulent	Turbulent
	Turb. model	k-epsilon
Advanced	Humidity	No

4.2. Simulation Results

In order to assess the accuracy and reliability of the CFD simulations, the base model's thermal distribution was compared to the CFD model from Hernandez-Perez et al. [28] (see Figure 5). The overall thermal distribution of the developed CFD model showed some degree of resemblance to the original model from the referenced study. Furthermore, the range of temperatures across the panels showed relatively close similarity, with the top-left corner being at roughly 38 °C and the bottom-left corner being at around 42 °C. It was determined through this validation process that the model was satisfactory.

**Figure 5.** CFD model validation [28].

Despite the base model showing similar results to the referenced paper, an inspection of the air around the same panel with no fins attached barely displayed any signs of a flow-separation bubble, as seen in Figure 6. While this initially cast doubts on the reliability of the CFD model, the absence of the air bubble was attributed to the fact that the air is approaching the panel from the back rather than from the front, especially since small pockets of hot air can still be seen trapped inside the edges of the panel frame.

A summary of the thermal performance for all the developed models can be seen in Figure 7. The base model with no perforations as well as a standard panel with no fins were also added for reference.

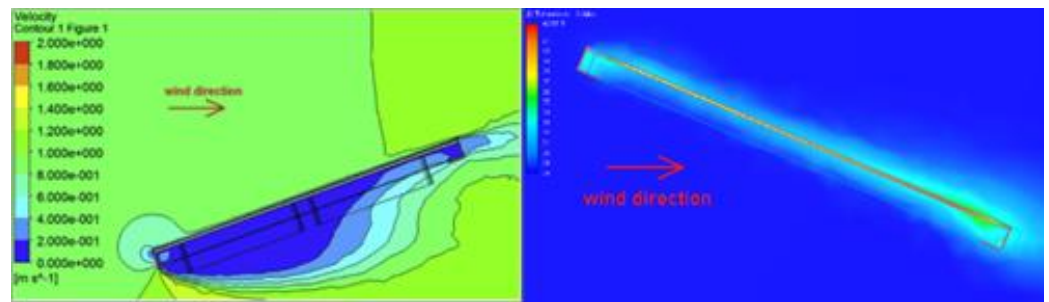


Figure 6. Flow-separation bubble from this study (right) compared to [25].

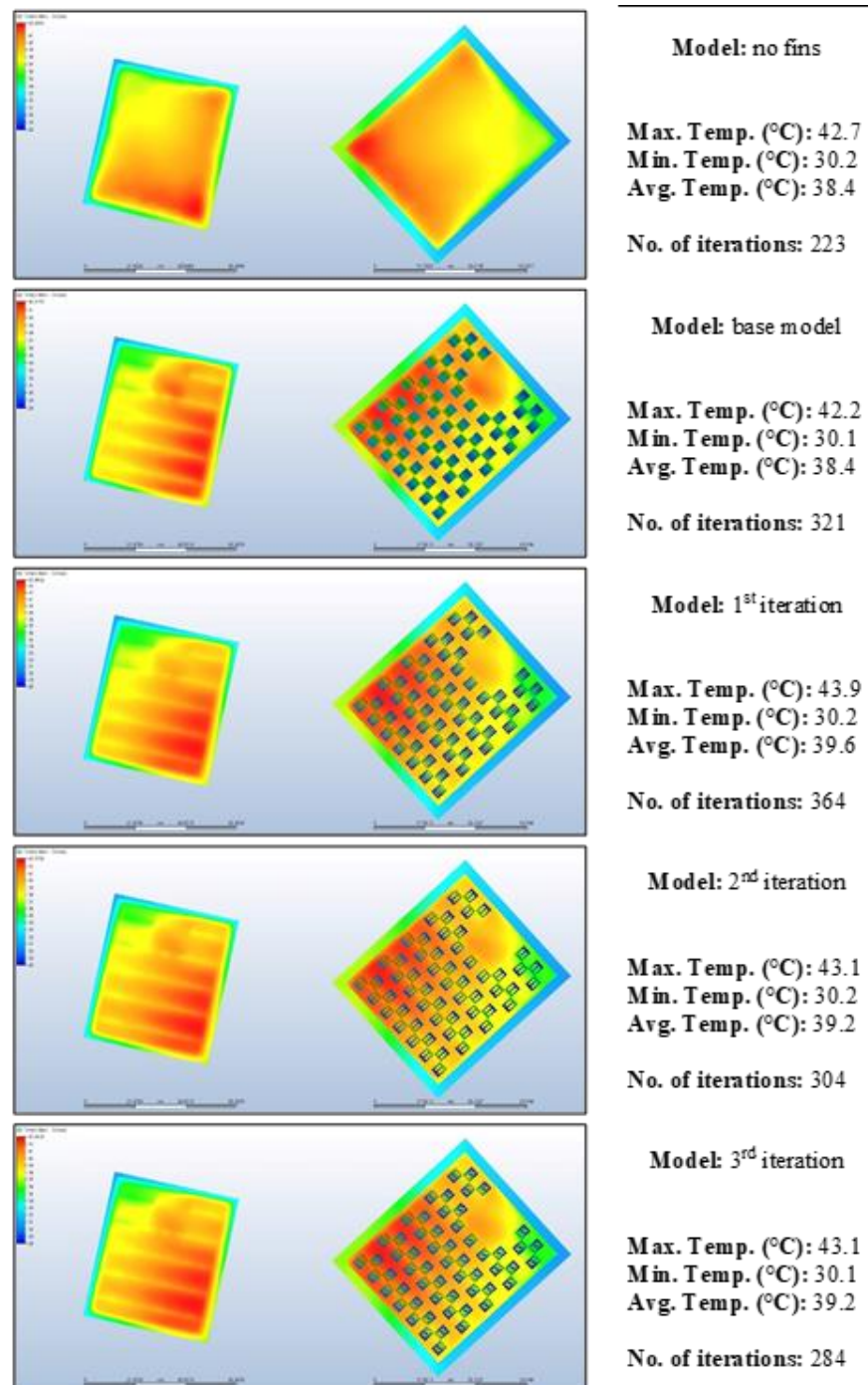


Figure 7. Cont.

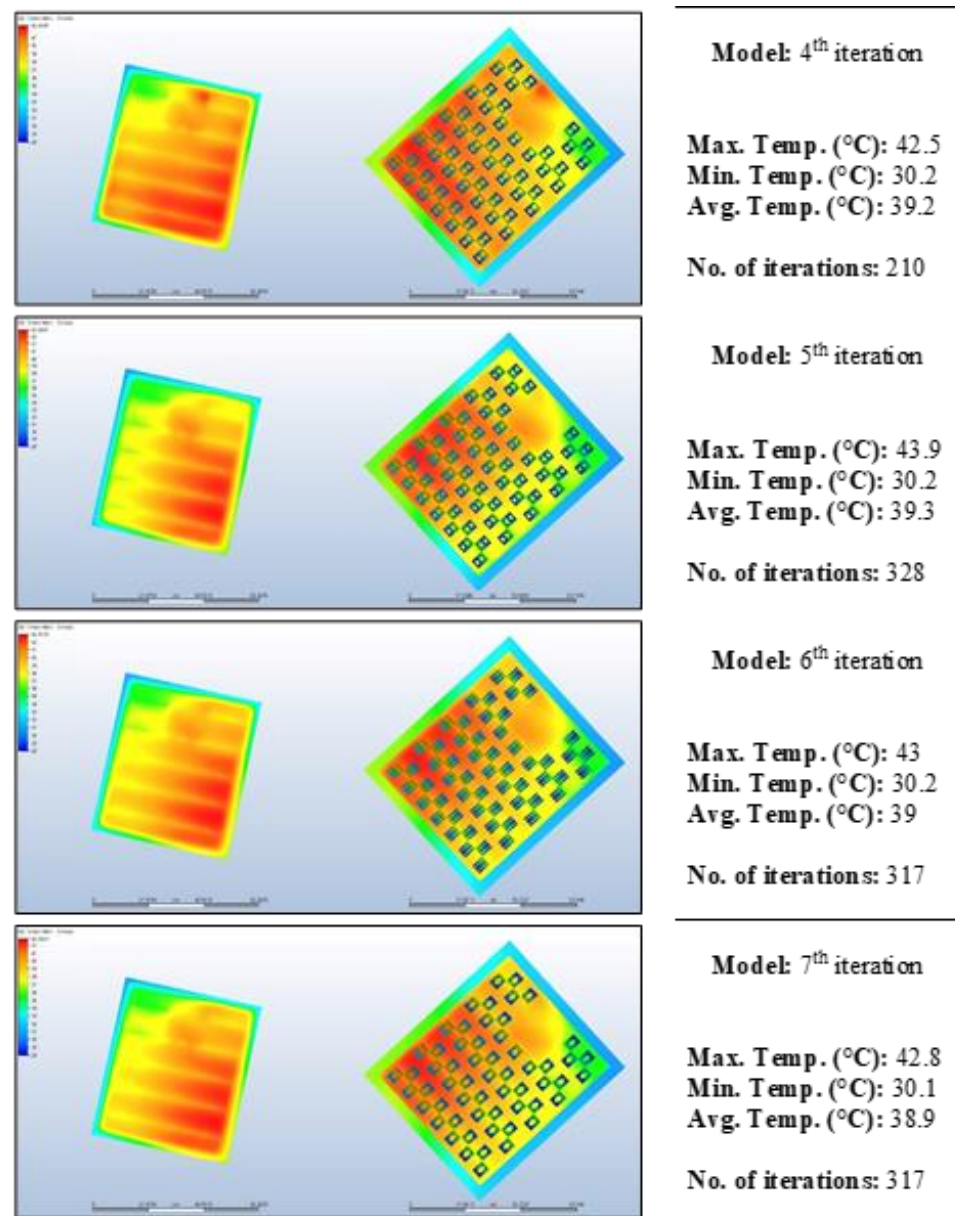


Figure 7. CFD model results.

A visual comparison of the thermal distribution across the seven different iterations developed showed that the fourth iteration had a relatively more homogenous temperature distribution. This was supported by the fact that the fourth iteration (Figure 8) exhibited the lowest maximum temperature amongst all the other iterations (42.5 °C). Compared to the other fin designs, the fourth iteration had a higher-than-average cut-out area (28.7%), coming only second to the second iteration, which possessed the largest cut-out area out of all the developed designs (33.7%). Nevertheless, the maximum temperature for the second iteration was 0.6 °C higher than the fourth iteration. One of the possible reasons behind this could be the fourth iteration's streamlined perforation design, though this is only speculative.

Although the fourth iteration's maximum temperature was lower than the PV panel with no fins installed, its temperature was observed to be slightly higher than that of the original model. It was subsequently decided to experimentally test both models under realistic operating conditions in order to confirm these results.

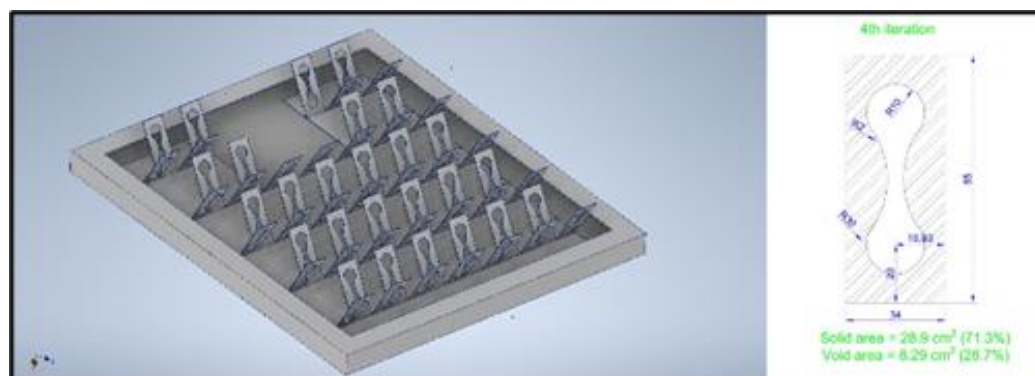


Figure 8. 3D model and fin dimensions of 4th iteration.

5. Experimental Study

5.1. Experimental Methodology

To evaluate the performance of the modified Al-fin heatsink against its precursor, both models were laser cut out of 22-gauge (0.71 mm) aluminium, which was the same thickness used in the original study (Table 4). These were then bent to the required $\pm 30^\circ$ angle. This was done manually, given that 22-gauge aluminium is relatively soft and does not require a substantial amount of force to bend. Thermally conductive adhesive tape was used instead of epoxy conductive glue so that the PV panel on which the heatsink is mounted can be used afterwards for other research purposes. While it was originally planned to use two identical panels where one of the panels serves as a control, as conducted by Grubisic-Cabo et al. [25] in their experimental study, it was only possible to use a single panel to carry out this experimental investigation. This was due to the unavailability of two panels of similar make and model in the research facility's inventory. The specifications of the PV panel used in this research can be seen in the following table:

Table 4. Working specifications of the solar panel.

Electrical Ratings at STC (1000 W/m ² , AM 1.5 Spectrum, Cell Temperature 25 °C)	
Model	HPS0050
Manufacturer	Hollandia Power Solutions
Type	Monocrystalline Silicon
Peak Power (Pmax)	50.0 W
Power Tolerance	0~+3%
Voltage (Vmp)	18.6 V
Current (Imp)	2.69 A
Open Circuit Voltage (Voc)	22.7 V
Short Circuit Current (Isc)	2.88 A
Minimum Bypass Diode	12 A
Maximum Series Fuse	10 A

The experimental study took place on the premises of Heriot–Watt University in Dubai Knowledge Park (25°06′08.7″ N 55°09′44.0″ E) (Figure 9). Since an actual roof could not be accessed for this study due to university protocols, the experiments had to be carried out on top of an outdoor elevated concrete platform with an approximate height of 0.8 m above ground. Being situated next to an empty plot of land, it was considered close enough to mimic an actual, unobstructed roof environment.



Figure 9. Experiment location.

The Si-mono PV panel used for this research was placed facing south at a tilt angle of 24° . Due to the unavailability of a mounting structure, the panel had to be placed directly on the concrete platform, although a timber block of height 0.1 m (later replaced by a concrete block of the same height) was used to raise the front end of the panel slightly to avoid contact between the fins and the ground.

The experiment was carried out over the course of three separate days (24, 28, and 30 March 2023), taking place at 2:19 p.m., 12:40 p.m., and 12:19 p.m., respectively. The skies were generally clear over the three days during which the study was carried out, with the exception of some intermittent cloud cover lasting for a few minutes. The panel's temperature was recorded at 30 s intervals over the duration of one hour for every day of the study. This was recorded using a temperature logger which was connected to two k-type thermocouples attached to the front and back of the panel, respectively, using the same thermally conductive tape used for mounting the Al-fins. These were each attached to the centres of the front and back of the panel, as seen in pictures from the experimental results. In addition to that, wind speed and temperature, as well as irradiance and ground temperature, were also recorded at 30 s intervals over the course of a full hour for each experiment day. Since these could not be connected to a data logger, the data had to be recorded manually. The measuring instruments used in the study can be seen below (Table 5).

Table 5. Measurement apparatus.

Measuring Instrument (Model)	Function
EXTECH SDL200 4-channel temperature meter	temperature logger ($^\circ\text{C}$ or K) (for k-type thermocouples)
Testo 480/425 Hotwire thermo-anemometer	measuring wind speed (m/s) and air temperature ($^\circ\text{C}$)
FLUKE IRR1-SOL	measuring solar irradiance (W/m^2), ambient and PV module temperature ($^\circ\text{C}$), array orientation and tilt angles ($^\circ$)
FLIR E40bx thermal imaging camera	thermal imaging

5.2. Experimental Results

Considering that the data for the experimental study had to be collected over separate days due to the unavailability of a referent panel, it was hard to effectively compare the performance of the two fin heatsinks to determine which one was the most viable and whether or not the introduction of perforations had any significant effect on the thermal performance of the PV panel. Nevertheless, it was still possible to deduce some key observations based on the available data.

It was very clear that the panel with no fins had a much higher temperature compared to the panels with heatsinks attached. This was evident by the 11°C difference in the

average panel-face temperature, despite the no-fin panel being subjected to much less irradiance and ambient temperatures. This is congruent with the results obtained by Hernandez-Perez et al. [28], which showed 9.4 °C as a result of using the segmented fin heatsink. This reduction in temperature would correspond to an increase in panel efficiency by approximately 5%, given that panel efficiency decreases by 0.25–0.5% for every 1 °C increase in temperature above the STC. On the other hand, while the ground temperature was rather high, the extreme panel-face temperature cannot be attributed to it, as it would have been more reasonable for the average back-panel temperature to show this increase, as well since it is more exposed to the ground. Table 6 and Figure 10 displays the detailed air temperature, velocity, and irradiance patterns obtained for the different fin configurations.

Table 6. Summary of experimental results.

Case	Date	Avg. Face (°C)	Avg. Back (°C)	Avg. Air Vel. (m/s)	Avg. Air Temp. (°C)	Avg. W/m ²	Avg. Ground Temp (°C)
No fins	24/03/2023	57.6	47.1	3.19	26.9	704	37.7
Base model	28/03/2023	46.6	45.5	3.10	29.8	932	38.6
4th iteration	30/03/2023	46.3	45.5	2.83	28.0	975	37.1

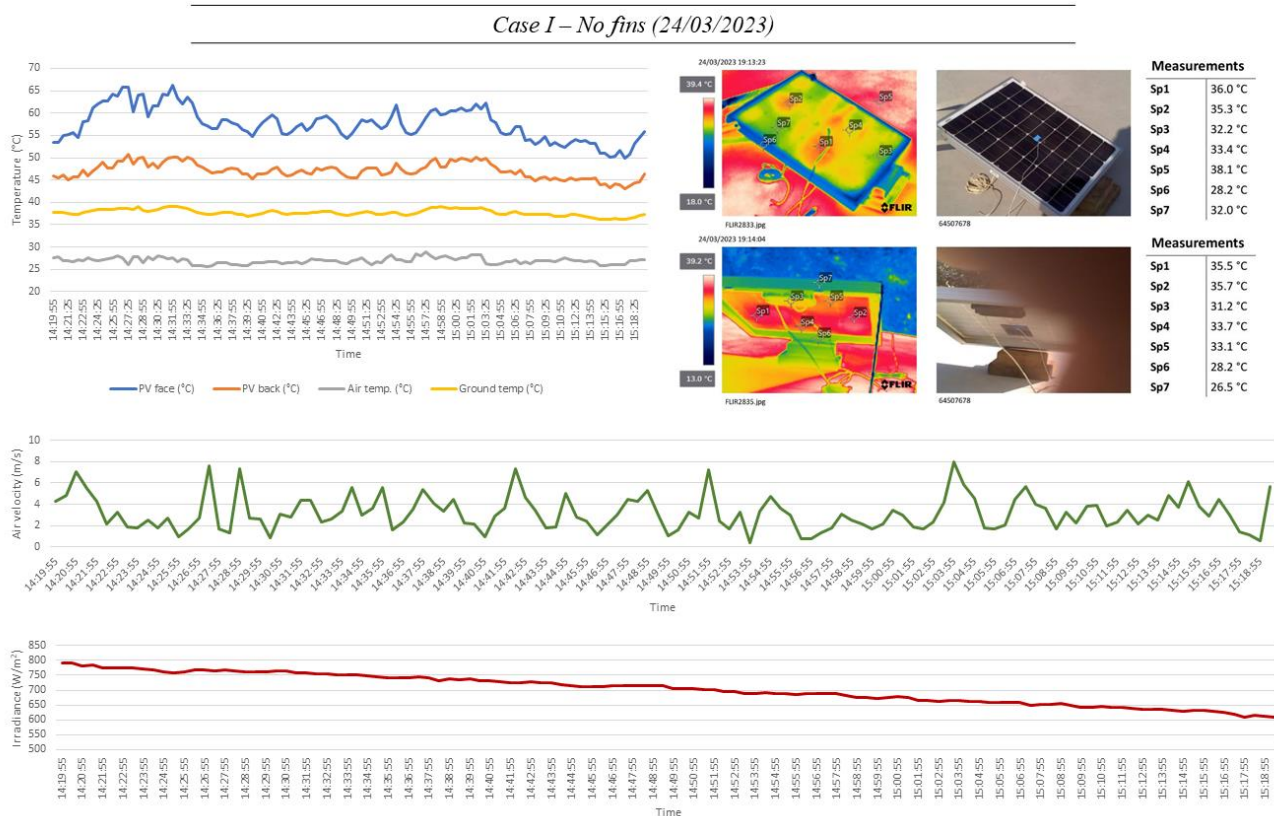


Figure 10. Cont.

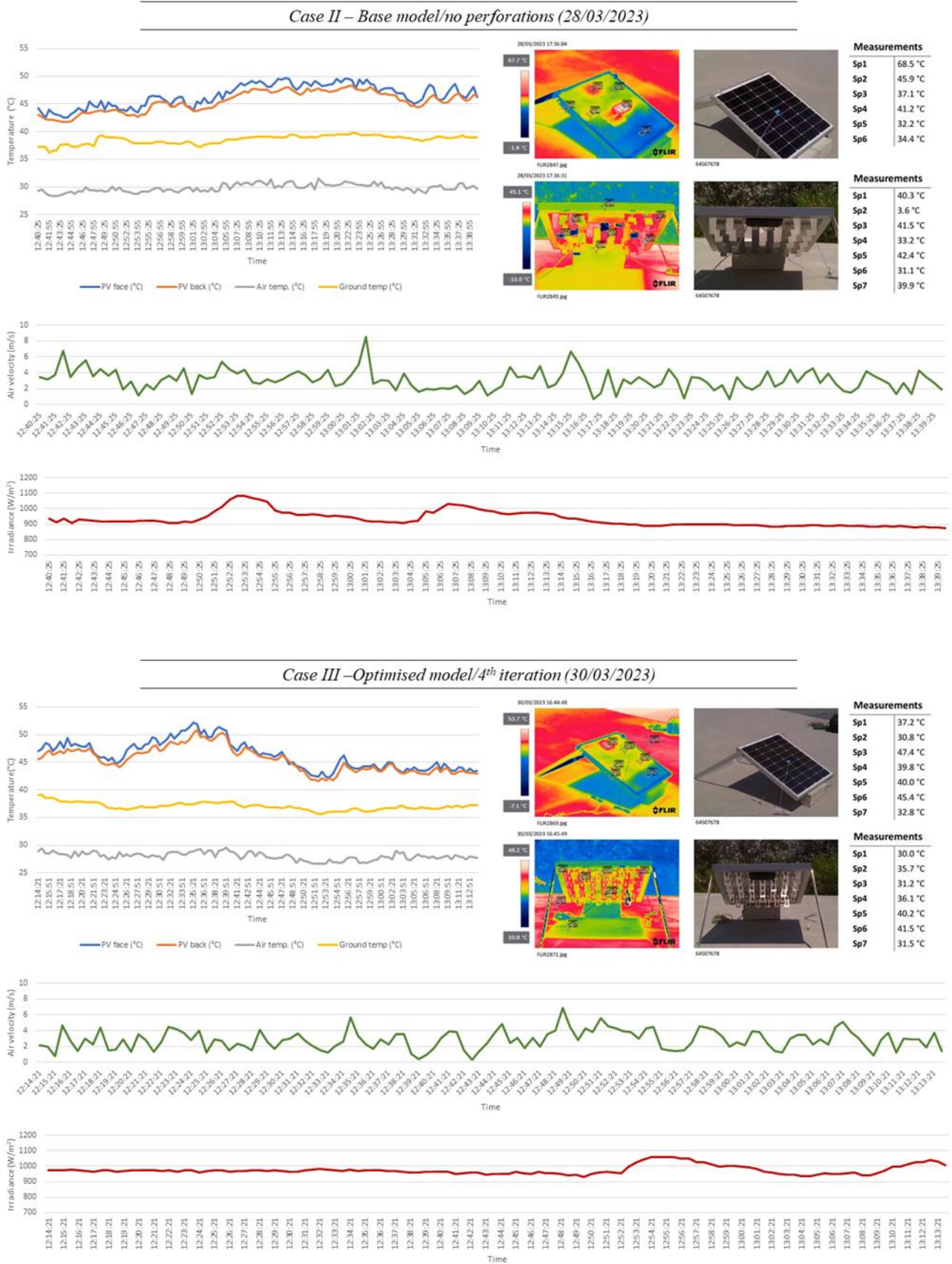


Figure 10. Air temperature, velocity, and irradiance analysis for the proposed fin configurations.

When it came to comparing the performance of the proposed model (fourth iteration), with the original model proposed by Hernandez-Perez et al. [28], it was rather difficult to tell whether the proposed model indeed outperforms the base model, as indicated by the 0.3 °C difference between the average face temperatures. Although the higher average air and ground temperatures can be used to argue that the base model was actually at a disadvantage in this study, the fact that the proposed model was still able to maintain good performance, given that it was subjected to greater irradiance and slower wind speeds, may indicate otherwise. However, it is hard to weigh the effect of each of the climatic factors involved in both cases to make an argument for either model due to the lack of sufficient data. It is also worth mentioning that the hotspots resulting from the attachment of thermocouples to the PV face could potentially be skewing the data. The issue of hotspots was actually recognised by Grubišić-Čabo et al. [24], who concluded that thermal imaging may be more reliable in terms of providing approximations of panel temperature, given the fact that every positioned thermocouple on the panel will inevitably result in the formation of hotspots. In spite of this, since the position of thermocouples was not changed as the same panel was used to test heatsinks, it is fair to assume that it had an equal effect on both sets of data.

Regardless of all this, even if the proposed model does not outperform the base model and only yields the same average temperature observed in the case of the back-panel temperature, the proposed model would still be deemed successful for yielding the same temperature reduction using fewer materials since this would directly translate to cost savings as well as a reduction in the weight of the system, especially when applied at a large scale.

6. Conclusions

The results of this study indicate that the PV cell temperature can be decreased by up to 10 °C with the placement of an aluminium fin heatsink, potentially resulting in a corresponding enhancement of approximately 5% in panel efficiency. With regards to optimizing the fin design, the findings established that the cut-out area of 28.7% yielded the highest temperature drop. Nonetheless, a comprehensive evaluation of the photovoltaic panel's electrical performance is required to confirm this estimated improvement.

Overall, while a final verdict cannot be made for the viability of fin design and perforations, the results obtained by this research still necessitate further investigation into the concept and its potential. Future studies may wish to investigate this in an actual roof environment and over a longer duration of time in order to obtain a larger set of data based on which conclusive evaluations could be made. It is also possible to further assess the economic aspect of utilising perforations, given that their implementation necessitates the use of laser-cutting machinery, which may incur significant costs in the case of such a solution being deployed on a large scale.

Author Contributions: Conceptualization, H.N.C. and T.A.; methodology, T.A.; software, T.A.; validation, T.A., H.N.C. and J.K.C.; formal analysis, T.A.; investigation, T.A.; resources, T.A.; data curation, T.A.; writing—original draft preparation, T.A.; writing—review and editing, H.N.C. and J.K.C.; visualization, T.A.; supervision, H.N.C.; project administration, H.N.C. All authors have read and agreed to the published version of the manuscript.

Funding: This research received no external funding.

Data Availability Statement: Data available on request due to restrictions.

Conflicts of Interest: The authors declare no conflict of interest.

References

1. Tricoire, J.-P. Why Buildings Are the Foundation of an Energy-Efficient Future. 2021. Available online: <https://www.weforum.org/agenda/2021/02/why-the-buildings-of-the-future-are-key-to-an-efficient-energy-ecosystem/> (accessed on 10 April 2023).
2. IEA. Buildings: Sectorial Overview. September 2022. Available online: <https://www.iea.org/reports/buildings> (accessed on 11 April 2023).

3. Fraunhofer ISE. Photovoltaics Report. Available online: <https://www.ise.fraunhofer.de/content/dam/ise/de/documents/publications/studies/Photovoltaics-Report.pdf> (accessed on 22 September 2022).
4. Li, H.; Zhao, J.; Li, M.; Deng, S.; An, Q.; Wang, F. Performance analysis of passive cooling for photovoltaic modules and estimation of energy-saving potential. *Sol. Energy* **2019**, *181*, 70–82. [CrossRef]
5. CHINT. Comprehensive Guide to Monocrystalline Solar Panel. 2023. Available online: <https://chintglobal.com/blog/monocrystalline-solar-panel/> (accessed on 11 April 2023).
6. Skoplaki, E.; Palyvos, J.A. On the temperature dependence of photovoltaic module electrical performance: A review of efficiency/power correlations. *Sol. Energy* **2009**, *83*, 614–624. [CrossRef]
7. Nazari, S.; Eslami, M. Impact of frame perforations on passive cooling of photovoltaic modules: CFD analysis of various patterns. *Energy Convers. Manag.* **2021**, *239*, 114228. [CrossRef]
8. Assadeg, J.A.; Fudholi, A.; Sopian, K.B. Performance of grid-connected solar photovoltaic power plants in the Middle East and North Africa. *Int. J. Electr. Comput. Eng.* **2019**, *9*, 3375–3383. [CrossRef]
9. Nižetić, S.; Grubišić-Čabo, F.; Marinić-Kragić, I.; Papadopoulos, A.M. Experimental and numerical investigation of a backside convective cooling mechanism on photovoltaic panels. *Energy* **2016**, *111*, 211–225. [CrossRef]
10. Abd-Elhady, M.; Serag, Z.; Kandil, H.A. An innovative solution to the overheating problem of PV panels. *Energy Convers. Manag.* **2018**, *157*, 452–459. [CrossRef]
11. Dida, M.; Boughali, S.; Bechki, D.; Bouguettaia, H. Experimental investigation of a passive cooling system for photovoltaic. *Energy Convers. Manag.* **2021**, *243*, 114328. [CrossRef]
12. Al-Shamani, A.N.; Yazdi, M.H.; Alghoul, M.; Abed, A.M.; Ruslan, M.; Mat, S.; Sopian, K. Nanofluids for improved efficiency in cooling solar collectors—A review. *Renew. Sustain. Energy Rev.* **2014**, *38*, 348–367. [CrossRef]
13. Nižetić, S.; Giama, E.; Papadopoulos, A. Comprehensive analysis and general economic-environmental evaluation of cooling techniques for photovoltaic panels, Part II: Active cooling techniques. *Energy Convers. Manag.* **2020**, *155*, 301–323. [CrossRef]
14. Vittorini, D.; Cipollone, R. Fin-cooled photovoltaic module modeling—Performances mapping and electric efficiency assessment under real operating conditions. *Energy* **2019**, *167*, 159–167. [CrossRef]
15. Nižetić, S.; Papadopoulos, A.; Giama, E. Comprehensive analysis and general economic-environmental. *Energy Convers. Manag.* **2017**, *149*, 334–354. [CrossRef]
16. Safi, T.S.; Munday, J.N. Improving photovoltaic performance through radiative cooling in both terrestrial and extraterrestrial environments. *Opt. Express* **2015**, *23*, A1120–A1128. [CrossRef] [PubMed]
17. Ahmad, E.Z.; Sopian, K.; Jarimi, H.; Fazlizan, A.; Elbreki, A.; Hamid, A.S.A.; Rostami, S.; Ibrahim, A. Recent advances in passive cooling methods for photovoltaic performance enhancement. *Int. J. Electr. Comput. Eng.* **2021**, *11*, 146–154. [CrossRef]
18. Hasan, A.; McCormack, S.; Huang, M.; Norton, B. Characterization of phase change materials for thermal control of photovoltaics using Differential Scanning Calorimetry and Temperature History Method. *Energy Convers. Manag.* **2014**, *81*, 322–329. [CrossRef]
19. Okogeri, O.; Stathopoulos, V.N. What about greener phase change materials? A review on biobased phase change materials for thermal energy storage applications. *Int. J. Thermofluids* **2021**, *10*, 100081. [CrossRef]
20. Maiti, S.; Banerjee, S.; Vyas, K.; Patel, P.; Ghosh, P.K. Self regulation of photovoltaic module temperature in V-trough using a metal-wax composite phase change matrix. *Sol. Energy* **2011**, *85*, 1805–1816. [CrossRef]
21. Tina, G.; Rosa-Clot, M.; Rosa-Clot, P.; Scandura, P. Optical and thermal behavior of submerged photovoltaic solar panel: SP2. *Energy* **2012**, *39*, 17–26. [CrossRef]
22. Abdulgafar, S.A.; Omar, O.S.; Yousif, K.M. Improving The Efficiency of Polycrystalline Solar Panel via Water Immersion Method. *Int. J. Innov. Res. Sci. Eng. Technol.* **2014**, *3*, 8127–8132.
23. Al-Amri, F.; Maatallah, T.S.; Al-Amri, O.F.; Ali, S.; Ali, S.; Ateeq, I.S.; Zachariah, R.; Kayed, T.S. Innovative technique for achieving uniform temperatures across solar panels using heat pipes and liquid immersion cooling in the harsh climate in the Kingdom of Saudi Arabia. *Alex. Eng. J.* **2022**, *61*, 1413–1424. [CrossRef]
24. Grubišić-Čabo, F.; Nižetić, S.; Kragić, I.M.; Čoko, D. Further progress in the research of fin-based passive cooling. *Wiley Int. J. Energy Res.* **2019**, *43*, 3475–3495. [CrossRef]
25. Grubišić-Čabo, F.; Nižetić, S.; Kragić, I.M.; Čoko, D. Experimental investigation of the passive cooled free-standing. *J. Clean. Prod.* **2018**, *176*, 119–129. [CrossRef]
26. Marinić-Kragić, I.; Nižetić, S.; Grubišić-Čabo, F.; Čoko, D. Analysis and optimization of passive cooling approach for free-standing photovoltaic panel: Introduction of slits. *Energy Convers. Manag.* **2020**, *204*, 112277. [CrossRef]
27. Nižetić, S.; Marinić-Kragić, I.; Grubišić-Čabo, F.; Papadopoulos, A.M.; Xie, G. Analysis of novel passive cooling strategies for free-standing silicon photovoltaic panels. *J. Therm. Anal. Calorim.* **2020**, *141*, 163–175. [CrossRef]
28. Hernandez-Perez, J.; Carrillo, J.; Bassam, A.; Flota-Banuelos, M. A new passive PV heatsink design to reduce efficiency losses: A computational and experimental evaluation. *Renew. Energy* **2020**, *147*, 1209–1220. [CrossRef]
29. Mankani, K.; Chaudhry, H.N.; Calautit, J.K. Optimization of an air-cooled heat sink for cooling of a solar photovoltaic. *Energy Build.* **2022**, *270*, 112274. [CrossRef]
30. ICF. Raw Materials Update. April 2017. Available online: https://www.icf.at/fileadmin/user_upload/News/2017/Issue_78_April_2017/ICF_NL_78-1704.pdf (accessed on 14 April 2023).
31. Bahaidarah, H.M.; Baloch, A.A.; Gandhidasan, P. Uniform cooling of photovoltaic panels: A review. *Renew. Sustain. Energy Rev.* **2016**, *57*, 1520–1544. [CrossRef]

32. Launder, B.E.; Spalding, D.B. *Lectures in Mathematical Models of Turbulence*; Academic Press: London, UK, 1972.
33. Ekambara, K.; Dhotre, M.T.; Joshi, J.B. CFD simulation of homogeneous reactions in turbulent pipe flows-Tubular non-catalytic reactors. *Chem. Eng. J.* **2006**, *117*, 23–29. [[CrossRef](#)]

Disclaimer/Publisher's Note: The statements, opinions and data contained in all publications are solely those of the individual author(s) and contributor(s) and not of MDPI and/or the editor(s). MDPI and/or the editor(s) disclaim responsibility for any injury to people or property resulting from any ideas, methods, instructions or products referred to in the content.